LA-UR -80-417

CCNF-791220--5

TITLE: EFFECT OF NONLINEAR REFRACTION ON BEAM BRIGHTNESS IN LASER FUSION APPLICATIONS

AUTHOR(S): Claude R. Phipps, Jr., David E. Watkins, and Scott J. Thomas

MASTER

SUBMITTED TO: Lasers '79 Conference, Orlando, FL, Dec. 15-20, 1979

DISCLAIMER

University of California

LOS ALAMOS SCIENTIFIC LABORATORY
Post Office Box 1663 Los Alamos, New Mexico 87545
An Affirmative Action/Equal Opportunity Employer

Form No. 836 R3
St. No. 2629
12/78

UNITED STATES
DEPARTMENT OF ENERGY
CONTRACT W-7405-ENG. 36

EFFECT OF NONLINEAR REFRACTION ON BEAM BRIGHTNESS IN LASER FUSION APPLICATIONS*

by

C. R. Phipps, Jr., S. J. Thomas and D. E. Watkins

University of California
Los Alamos Scientific Laboratory
Los Alamos, NM 87544

Abstract

The far-field brightness loss due to nonlinear refraction of a laser beam of finite transverse extent is a limitation for phase conjugation. We present exact calculations, supported by measurements, for these effects in Gaussian beams.

Introduction

Nonlinear refraction is a familiar consideration in the optical design of most high-power, short-pulse laser systems.[1] Practical laser beams must be apodized in some fashion, and the apodization leads to intensity-dependent lensing in material media which can seriously degrade the far-field pattern which the system would otherwise produce. Even in high-power gas lasers, where the nonlinear susceptibility of the laser medium is ordinarily quite small, brightness loss can be significant in a single window.

Such effects have been largely ignored in the initial treatments of phase conjugation via degenerate four-wave mixing (DFWM) although one of the major present applications is to phase and pointing correction in high-power lasers. In one class of such proposals[2], a large third-order optical nonlinearity identical to that which causes self-focusing is relied upon to produce the conjugate wave efficiently, while the schemes which avoid relying solely upon large real nonlinear susceptiblity[3] are apt to be limited by the same effects in their practical application.

This limitation arises from the fact that the product of pump-beam intensity and optical path length required for efficient phase conjugation is similar to that which can, in certain instances, cause sufficient pump wavefront distortion to degrade reconstructed wave quality.

In order to illustrate this point, consider the relationship between the coupling coefficient K, which figures in phase-conjugate reflectivity,

$$R = \tan^2 (KL) \tag{1}$$

and the phase change ϕ which occurs due to the propagation of one of the pumps at the intensity required to produce a given reflectivity. For the sake of simplicity, assume an isotropic lossless material of length L with nonlinear index n_2. The refractive index change is

$$n(z)-n_o = \Delta n(z) = n_2 < E^2(z,t) >_t \tag{2}$$

and the corresponding phase retardation is given by

$$\phi = \int_o^L dz\ k_o\ \Delta n(z) \tag{3}$$

(where $k_o = \omega/c$) for a given electric field distribution. For a single wave with amplitude E_1, Eq. 2 gives $\Delta n = 1/2\ n_2 E_1^2$. However, in the case corresponding to DFWM, two counterpropagating, monochromatic, infinite plane waves of equal amplitude E_1 together produce a standing refractive index grating, $\Delta n(z) = 2n_2 E_1^2 \cos^2(k_o n_o z)$. From Eq. 3, the phase change seen by each wave in this case is twice as great on the average as that for one wave alone,

$$\phi \approx k_o n_2 E_1^2 L = KL \tag{4}$$

and is equal to the product[5] KL.

From Eq. 1, the conditions necessary to give a 50% conjugate reflectivity will also alter the phase of each pump wave by 0.62 ≈ π/5 radians on passing through the sample.

*Work performed under the auspices of the U. S. Department of Energy.

Phase conjugation by DFWM is analogous to reconstruction of a volume hologram with a reversed or "conjugate" reference wave. When apodized pump waves are used, the distortion we have just estimated is present as a curvature in both pumps, and additive in the sense that the "reconstruction" beam has its curvature reversed relative to what one would desire in order to recreate a perfect "conjugate image" of a third, probe (object) wave.[5]

Although the case for apodized pumps is somewhat more complicated in detail than that described in the preceding simple analysis, once significant wavefront distortion has occurred, we may estimate a distortion of the conjugate wavefront equal to $2\emptyset = 0.4\pi$ radians ($\lambda_o/5$ in free space) arising from nonlinear refraction of the pumps when K is totally real and R = 50%.

One reason for ignoring this effect has been the lack of simple analytical and experimental models for determining the dependence of wavefront distortion on intensity for specific apodizations. It is the purpose of this paper to report an extension of earlier work[1,7] giving a complete description of the far-field intensity distribution which results from nonlinear refraction occurring in the near-field of a general hypergaussian profile beam. The form of this result is sufficiently simple to permit easy numerical integration over time, radius or both in the far field, and thereby give direct comparisons with measurements of encircled power or energy. These relationships are especially easy to use when the intensity profile is that of a normal Gaussian, even when a Gaussian time variation is present in the laser pulse.

We will first develop the general hypergaussian solution, then specialize to the Gaussian case and give experimental examples which are well described by these results. We will show that, in many cases, the far-field brightness loss is an extremely sensitive way of measuring the nonlinear index.

Far-Field Pattern of a Hypergaussian Beam in a Thin, Optically Nonlinear Window

We assume an axisymmetric electric-field amplitude distribution of the form:

$$E(r,0-)/E_o = \exp[-ar^p] \quad , \; p \geq 2 \; , \; a = (1/w)^p \tag{5}$$

incident on a thin anti-reflection coated, transparent window of isotropic nonlinear material with thickness L. If the window is sufficiently thin, it will impart only a phase distribution to the exit beam, so that

$$E(r,L+)/E_o = \exp[-ar^p + iB\exp(-2ar^p)] \quad . \tag{6}$$

Since the intensity[1] $I = cnE^2/8\pi$ is conserved across an anti-reflection coated interface, the internal (E_1) and external (E_o) fields are related by $E_1 = E_o/\sqrt{n}$, and from Eqs. 2 and 3, the parameter B is related to the other variables by:

$$B = k_o n_2 E_1^2 \, L/2 = k_o n_2 E_o^2 \, L/2n \quad . \tag{7}$$

B is the phase shift produced in the center of the beam by nonlinear refraction, and is sometimes called the "beam breakup parameter." To convert from esu to practical units (W/cm^2), we write

$$B = k_o \hat{n}_2 I_o L/n_o \; , \tag{7a}$$

assuming $\Delta n \ll n_o$, with $\hat{n}_2(cm^2/W) = (4\pi \times 10^7/c)\, n_2(esu)$.

The window is sufficiently thin for the approximations involved in Eq. 6 to be valid when the typical change in ray direction within the sample, $\delta = (B/2\pi)(\lambda_o/n)/w$ is much less than w/L, or the Fresnel number

$$nw^2/L\lambda_o \gg B/2\pi \quad . \tag{8}$$

For a 1-cm-diameter CO_2 beam in Ge, for example, with B = 10, we require only that $L \ll 590$ cm.

The limitation set by the growth of small-scale instabilities in the beam profile is a more serious one even for CO_2 wavelengths. The quantities of interest here are the transverse spacial frequency $K_m = 2\pi/\lambda_m$ for the ripples with largest growth rate, and the axial gain g_m experienced by these ripples. The predictions of the linearized plane-wave theory for this problem[8] can be expressed in the form:

$$g_m = B/L, \; K_m = \sqrt{k_o g_m} \quad . \tag{9}$$

Eq. 9 shows that small-scale instability growth poses a limitation on B rather than L. Although we would expect that this theory would only apply for $K_m >> \pi/w$ in the present problem, it is clear that we should be alert for difficulties unless $B \lesssim 5$.

With the aid of a lens which is assumed optically linear and perfect, we can map the far field onto a plane at a finite distance f for convenient observation, as in Fig. 1.

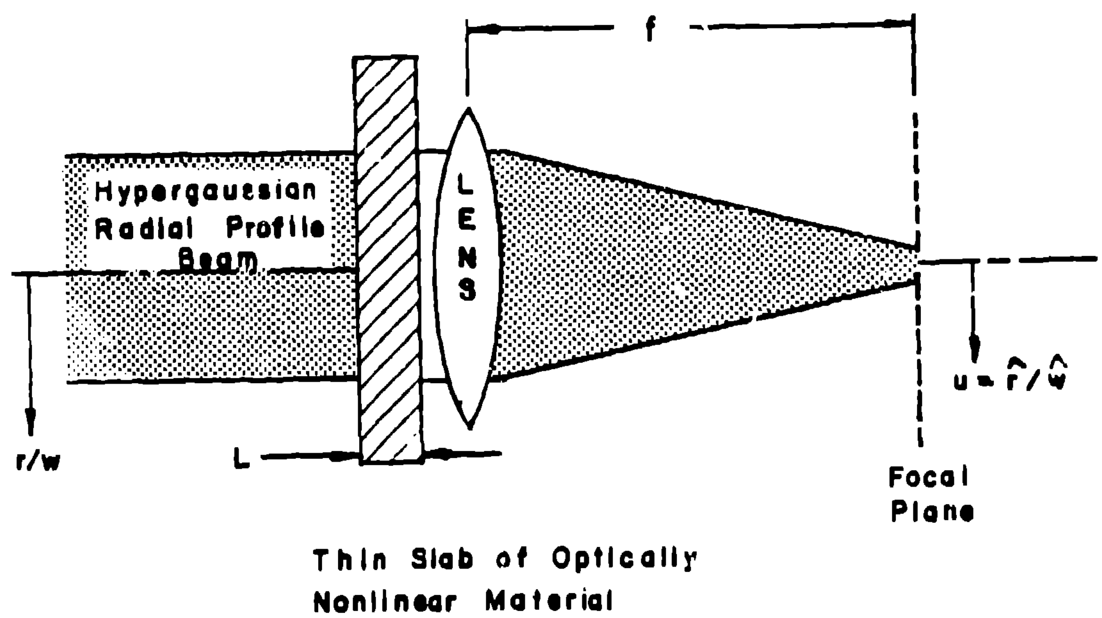

Figure 1. Conceptual Arrangement for Studying the Far-Field Pattern

The field at the lens focal plane is the axisymmetric spacial Fourier Transform (Hankel Transform) of the field produced by the window. In terms of the field of Eq. 6, $f(r) = E(r,L+)/E_0$, and the normalized focal plane radial coordinate $\hat{r} = k_0 r_f/f$, the focal plane field $g(\hat{r}) = E(\hat{r})/E_f$ is[9]:

$$g(\hat{r}) = 2\pi \int_0^\infty dr\; r\; f(r)\; J_0(r\hat{r}) = h\left\{f(r)\right\}. \tag{10}$$

To find the Hankel Transform of each one of the hypergaussian elements of the series expansion of Eq. 6, we employ the moment theorem to find

$$h\left\{e^{-mar^p}\right\} = 3\pi \sum_{n=0}^{\infty} \frac{(-1)^n m_{2n+1} \hat{r}^{2n}}{(n!)^2\, 2^{2n}}$$

where[10]

$$m_n = \int_0^\infty dr\; r^n\, e^{-mar^p} = \frac{1}{p}\,(ma)^{-(n+1)/p}\;\Gamma\!\left(\frac{n+1}{p}\right)$$

so that

$$h\left\{e^{-mar^p}\right\} = \frac{2\pi}{p} \sum_{n=0}^{\infty} \frac{(-1)^n\, \hat{r}^{2n}\; \Gamma\!\left(\frac{2n+2}{p}\right)}{2^{2n} (n!)^2\, (ma)^{(2n+2)/p}} \tag{11}$$

Now from Eq. 6, with $a = (1/w)^p$,

$$f_p(r) = \sum_{k=0}^{\infty} \frac{(iB)^k}{k!}\, e^{-(2k+1)(r/w)^p} \tag{12}$$

so that, defining $\hat{w} = (2/w) = 2a^{1/p}$, and $u = (\hat{r}/\hat{w})$, and using Eq. 11 to transform Eq. 12 term by term, we have:

$$g_p(\hat{r}) = \frac{2\pi w^2}{p} \sum_{k=0}^{\infty} \frac{(iB)^k}{k!} \sum_{n=0}^{\infty} \frac{(-1)^n\; u^{2n}\; \Gamma\!\left(\frac{2n+2}{p}\right)}{(n!)^2\, (2k+1)^{(2n+2)/p}} \tag{13}$$

Finally, to form the intensity $g_p(\hat{r})\, g_p^*(\hat{r})$ we use the relationship[11]

$$\sum_{k=o}^{\infty} a_k x^k \quad \sum_{k=o}^{\infty} b_k x^k = \sum_{k=o}^{\infty} x^k \sum_{m=o}^{k} a_m b_{k-m}$$

repeatedly to find:

$$|g_p(\hat{r})|^2 = C\left\{\sum_{k=o}^{\infty} (-B^2)^k \sum_{m=o}^{2k} \frac{(-1)^m}{m!(2k-m)!(4k-2m+1)^{2/p}\ (2m+1)^{2/p}} \right. \tag{14}$$

$$\left. \cdot \sum_{\ell=o}^{\infty} (-u^2)^{\ell} \sum_{s=o}^{\ell} \frac{\Gamma[\frac{2}{p}(s+1)]\,\Gamma[\frac{2}{p}(\ell-s+1)]}{\Gamma^2(s+1)\ \Gamma^2(\ell-s+1)\ [(4k-2m+1)^{2/p}]^{(\ell-s)}[(2m+1)^{2/p}]^s}\right\}$$

The constant $C = 1/\Gamma^2(2/p)$ is chosen so that $\lim_{B\to o} |g_p(o)|^2 = 1$.

Alternatively, Eq. 14 may be written in a simpler form that also leads to more convenient numerical computation when explicit radial integration is not required. This is:

$$|g_p(\hat{r})|^2 = C\left\{\left[\sum_{k=o}^{\infty} \frac{(-B^2)^k}{(2k)!} \sum_{m=o}^{\infty} \frac{(-u^2)^m\ \Gamma[\frac{2}{p}(m+1)]}{(m!)^2\ (4k+1)^{(2/p)(m+1)}}\right]^2 \right. \tag{14a}$$

$$\left. + \left[B \sum_{k=O}^{\infty} \frac{(-B^2)^k}{(2k+1)!} \sum_{m=o}^{\infty} \frac{(-u^2)^m\ \Gamma[\frac{2}{p}(m+1)]}{(m!)^2\ (4k+3)^{(2/p)(m+1)}}\right]^2\right\}$$

Specialization to the Normal Gaussian

When $p=2$, Eqs. 14 take on a much simpler form, given by

$$|g_2(\hat{r})|^2 = \sum_{k=o}^{\infty} (-B^2)^k \sum_{m=o}^{2k} \frac{(-1)^m \exp\left\{-\left[\frac{2(2k+1)}{(2m+1)\ (4k-2m+1)}\right]u^2\right\}}{m!\ (2k-m)!\ (4k-2m+1)\ (2m+1)} \tag{15}$$

and

$$|g_2(\hat{r})|^2 = \left\{\left[\sum_{k=o}^{\infty} \frac{(-B^2)^k}{(4k+1)(2k)!} e^{-u^2/(4k+1)}\right]^2 + \left[B \sum_{k=o}^{\infty} \frac{(-B^2)^k}{(4k+3)\,(2k+1)!} e^{-u^2/(4k+3)}\right]^2\right\} \tag{15a}$$

On axis,

$$|g_2(0)|^2 = \left[\sum_{k=o}^{\infty} \frac{(-B^2)^k}{(4k+1)\ (2k)!}\right]^2 + \left[B \sum_{k=o}^{\infty} \frac{(-B^2)^k}{(4k+3)\ (2k+1)!}\right]^2$$
$$= \frac{\pi}{2B}\left[C_2^2(B) + S_2^2(B)\right] \tag{16}$$

where C_2 and S_2 are the Fresnel integrals,

$$C_2(z) = \frac{1}{\sqrt{2\pi}} \int_0^z \frac{\cos t}{\sqrt{t}}\,dt \qquad\qquad S_2(z) = \frac{1}{\sqrt{2\pi}} \int_0^z \frac{\sin t}{\sqrt{t}}\,dt\ . \tag{17}$$

Eq. (17) was presented earlier by Marburger.

Relationship to the Airy Distribution

In the limit $[p \to \infty, B \to 0]$

$$|g_p(\hat{r})|^2 \longrightarrow \left[\sum_{m=0}^{\infty} \frac{(-u^2)^m}{(m+1)\ (m!)^2}\right]^2 = \left[\frac{2\ J_1(2u)}{(2u)}\right]^2 = \left[\frac{2\ J_1(\hat{r}w)}{(\hat{r}w)}\right]^2 \quad . \tag{18}$$

which is the appropriately normalized Airy distribution we would expect to find in the focal plane in the absence of nonlinear optical effects, due to a uniformly illuminated lens pupil of diameter 2w.

Encircled Energy or Power

Eq. 14 was presented to provide a means for explicitly forming the radial integral to some limit u_o, in order to determine the fraction of total energy or power encircled by a focal-plane iris of given radius. It is clear that this can be done, at least numerically, since Eq. 14 is a single series in powers of the intensity (B) and of the radius (u), permitting temporal and/or radial integration. However, the explicit form of these integrals for general p is not especially instructive.

However, when p=2, the Gaussian beam solution given by Eq. 15 may be integrated directly to give:

$$W_2(u\ ) = \frac{\int_0^{\hat{r}/\hat{w}=u_o} d\hat{r}\ 2\pi\hat{r}|g_2(\hat{r})|^2}{\int_0^{\infty} d\hat{r}\ 2\pi\hat{r}|g_2(\hat{r})|^2} = 1 + \sum_{k=0}^{\infty} \frac{(-B^2)^k}{(2k+1)} \sum_{m=0}^{2k} \frac{(-1)^{(m+1)} \exp\left[\frac{-2(2k+1)u_o^2}{(2m+1)(4k-2m+1)}\right]}{m!\ (2k-m)!} \tag{19}$$

for the fraction of total focal plane energy contained within the normalized radius u_o.

Temporal integration of Eqs. 14, 15 or 19, is readily performed. We note that since these relationships, as well as Eq. 6, are dimensionless (transmission-like), it is necessary to multiply the quantity by an additional power of intensity prior to time-averaging. If $B = B_o f(t)$, for example,

$$<|g_p\ (\hat{r},t)|^2>_t = \left\{\frac{\int_{-\infty}^{\infty} dt\ \ |g_p(\hat{r},t)|^2\ \ B(t)}{\int_{-\infty}^{\infty} dt\ B(t)}\right\} \tag{20}$$

In every case, then, time averaging comes down to replacing B^{2k} in the particular sum by $B_o^{(2k+1)} \int_{-\infty}^{\infty} f^{(2k+1)}(t)\ dt$, and renormalizing by the quantity $[B_o \int_{-\infty}^{\infty} f(t)dt]$. As an example, if $f(t) = 2^{-(t/\tau)^2}$

then

$$B^{2k} \longrightarrow \frac{B_o^{\ 2k}}{\sqrt{2k+1}} \tag{20a}$$

in Eqs. 14, 15 or 19 is equivalent to performing the time average of that expression over a laser pulse with a Gaussian time variation.

The Importance of Beam Profiles

Because the set of hypergaussian functions smoothly spans the range from a simple Gaussian radial distribution to a "hard-apertured" beam via adjustment of a single index, it is useful in the present context for assessing the impact of nonlinear refraction on the far-field pattern of practical laser devices.

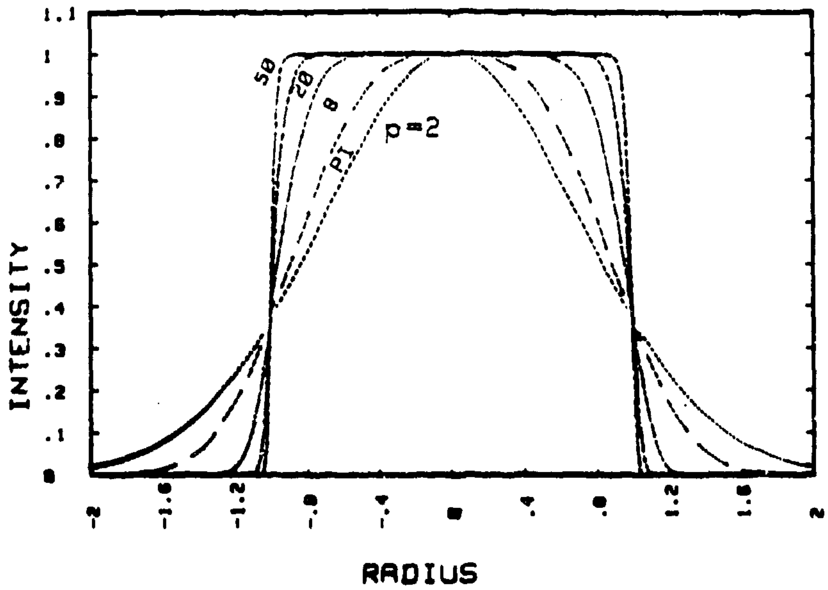

Figure 2. Hypergaussian Intensity Distributions for p = 2, π, 8, 20 and 50

Using the preceding relationships, it is easy to show that the near-field distributions of Fig. 2 are markedly different in regard to the sensitivity of their corresponding far-field distributions to increasing B. For example, Fig. 3 and 4 show the normalized far-field radial distributions calculated for p=2 and p=20, respectively, as B varies from 1 to 10. In both figures, the normalization described in connection with Eq. 14 is used, for unit on-axis intensity in the absence of nonlinear effects.

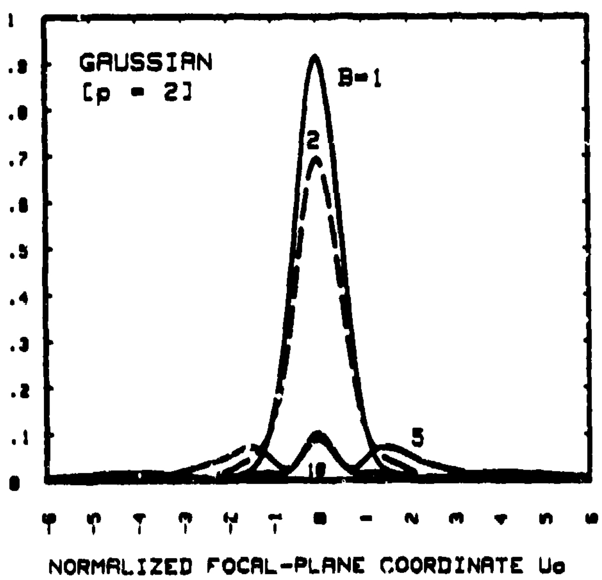

Figure 3. Calculated Far-Field Distributions for a Gaussian Beam as B Varies from 1 to 10.

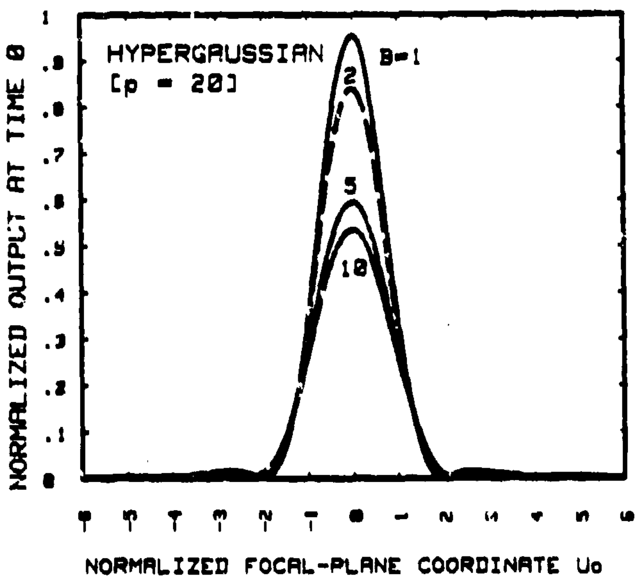

Figure 4. Far-Field Distributions as in Fig. 3, but for p=20.

The Strehl ratio[12], by which the central intensity in the far-field distribution is related to that which would exist in the absence of aberrations, is better than 50% in the second case, even for B=10, but is reduced nearly six-fold for a simple Gaussian beam under the same conditions. In some cases, e.g., p = π and B = 5.18, a zero Strehl ratio is obtained. Further details regarding on-axis intensities are provided in Ref. 13.

Although it is convenient for many experimental purposes to employ a beam with an accurately Gaussian transverse profile, this shape is very nearly a worst case for nonlinear refractive effects in the far field. The implications of these results depend upon whether it is desired to maximize or minimize these effects. In the remainder of this discussion, it is assumed that we wish to find experimental conditions that sensitively indicate nonlinear refraction, in order to provide a means of measuring nonlinear index, and that the foregoing discussion will be used to show how to minimize their impact in laser systems.

The Effect of Time- and Space-Averaging

The quantities we are most often interested in studying are seldom peak temporal or spacial intensities, but rather time- or space-averages, as, for example, the total energy encircled by a far-field aperture of given size during a laser pulse. Having picked a Gaussian profile beam as the most easily realized profile which provides good sensitivity to nonlinear index, and assuming also a Gaussian-shaped pulse, Fig. 5 compares the sensitivity of four different permutations of time-averaging or instantaneous detection methods and on-axis or radially-averaged focal-plane quantities, using the geometry of Fig. 1.

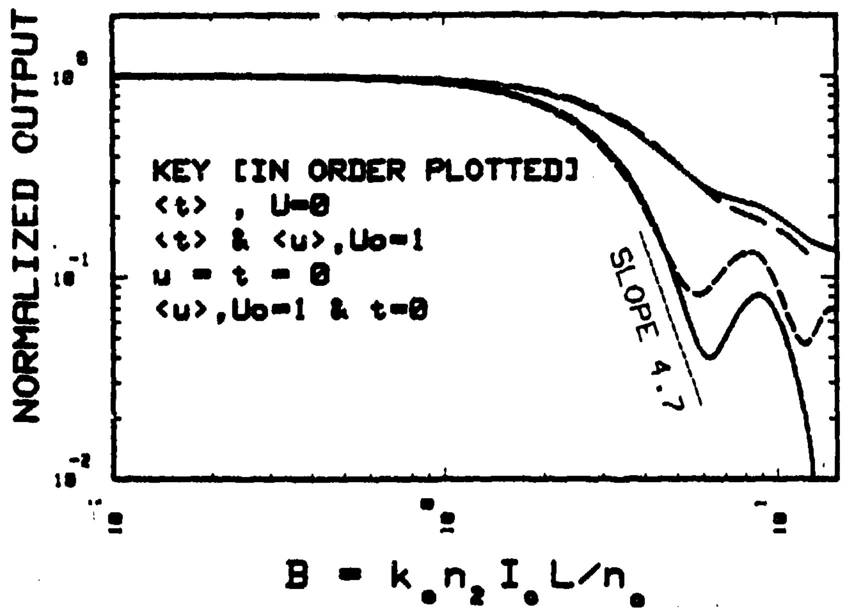

Figure 5. Calculations showing that, for a Gaussian spacetime beam, the most sensitive measurement scheme among the four studied involves recording the peak power transmitted by a focal plane iris with diameter equal to the beam waist of the linear optical distribution, while calorimetric measurements on axis are the least sensitive.

Experimental Applications of the Analysis

Figure 6 shows the generic experimental setup we employed in demonstrating agreement between experiment and theory, and in using this agreement to determine the nonlinear index of some materials, by using n_2 as the only free parameter. The Fig. 1 geometry is located to the right of the sample in the figure. Calibrated attenuators were optically flat and wedge-free plates of CaF_2. The CO_2 laser source has been described elsewhere.[14]

In particular, the beam in the experiment region is itself derived from the central part of the far-field distribution produced by the laser, so that its transverse profile is accurately Gaussian down to the 1-2% intensity points, extremely smooth compared to typical near-field beams, and essentially diffraction-limited in its own far field.

In all measurements, a 33-cm focal length, anti-reflection coated ZnSe lens was used to produce a focal plane distribution with 300-μm small-signal $1/e^2$ diameter. A centrally-located iris of the same size was used to obtain radially-averaged signals, while intensity-dependent Strehl measurements were made with a much smaller aperture within which the small-signal radial intensity variation was only +15%.

The detection system consisted of pyroelectric detectors and a LASL-built, channel-plate-intensified oscilloscope. The detection system electrical bandwidth is about 3 GHz,[15] giving a detection risetime at least 10 times faster than that of the 2-ns FWHM laser pulses employed.

When time-averaging of the detected signals was required, this was accomplished by numerically integrating the detected signals, rather than via the calorimeters shown, for best experimental accuracy. The calorimeters were used to monitor sample transmission T, in the relationship $L_{eff} = (1-T)/\alpha$, where α is the measured absorption coefficient.

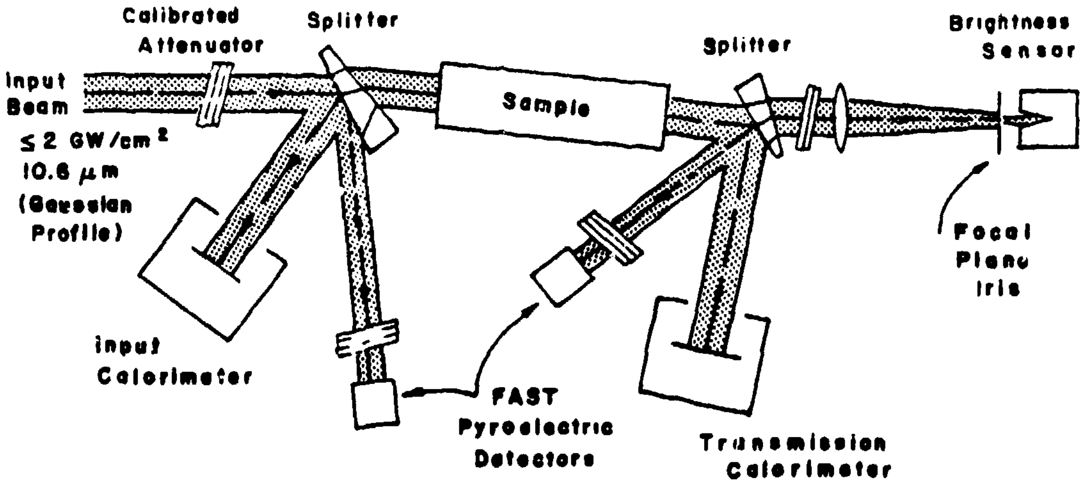

Figure 6. Experimental Setup

To test the absolute agreement between this and more fundamental methods of measuring nonlinear index, two anti-reflection coated, monocrystalline, intrinsic Ge boules were used. One of these was the same boule employed in reference 16, where the 10-μm nonlinear susceptibility was first measured via ellipse rotation. The samples were oriented so as to give an n_2 determination which would correspond to X_3^{1111}. For the greatest total sample length employed, the Eq. 8 inequality was satisfied in the ratio 66:1, while B values greater than 7.5 were not employed. In this case the time-averaged intensity-dependent Strehl was measured.

It will be seen from Fig. 7 that the agreement obtained between the data and the model is extremely good, and that mutual agreement was obtained between the two sets of data, for sample lengths covering a 3:1 range. This was the greatest range we could use without unduly attenuating the beam at one extreme, or reaching the plasma formation threshold at the other.[17] The result of this one-free-parameter study gave absolute agreement with the reference 16 measurement, to within a factor of two.

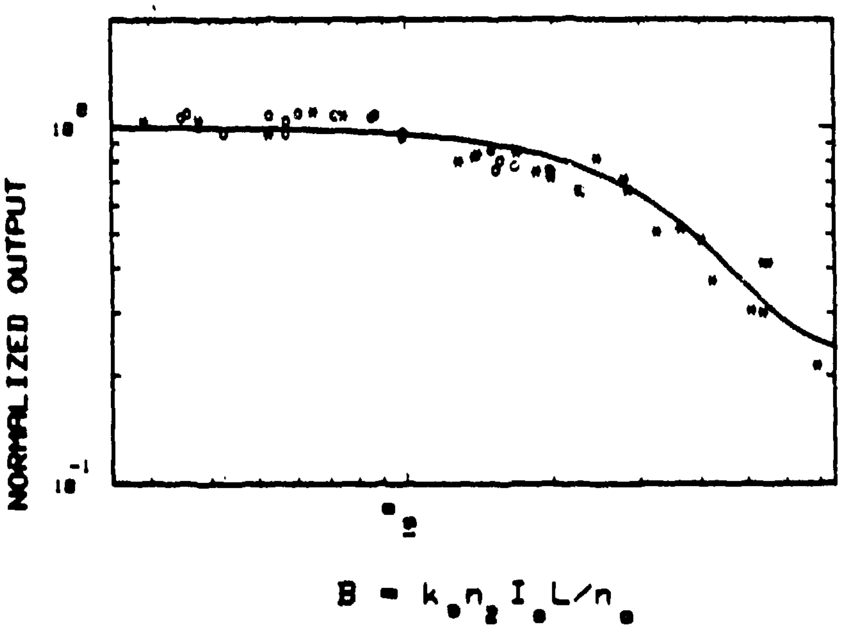

Figure 7. Measured time average relative brightness loss in the central zone of the far field vs. B for L=5.7 cm (o) and L=17.9 cm(*) using intrinsic Ge. The value of n_2 used in this case was 0.0026 cm^2/GW, which corresponds to X_3^{1111} = 6.5 x 10^{-11} esu, in factor-of-two agreement with ref. 16.

To demonstrate the relative effects of space- and time-averaging experimentally, we used a different boule of the same material, 14.2 cm in length. As shown in Fig. 8, a different crystal orientation produced a somewhat smaller nonlinear index. In this case the threshold for (reversible) plasma formation was deliberately exceeded on the last three laser shots. Here, the most sensitive measurement configuration shown in Fig. 5 was studied, and compared to the time-average of that data. In the former, the power transmitted by the 300-um focal plane iris at a time corresponding to the input pulse peak is recorded for increasing values of B_o.

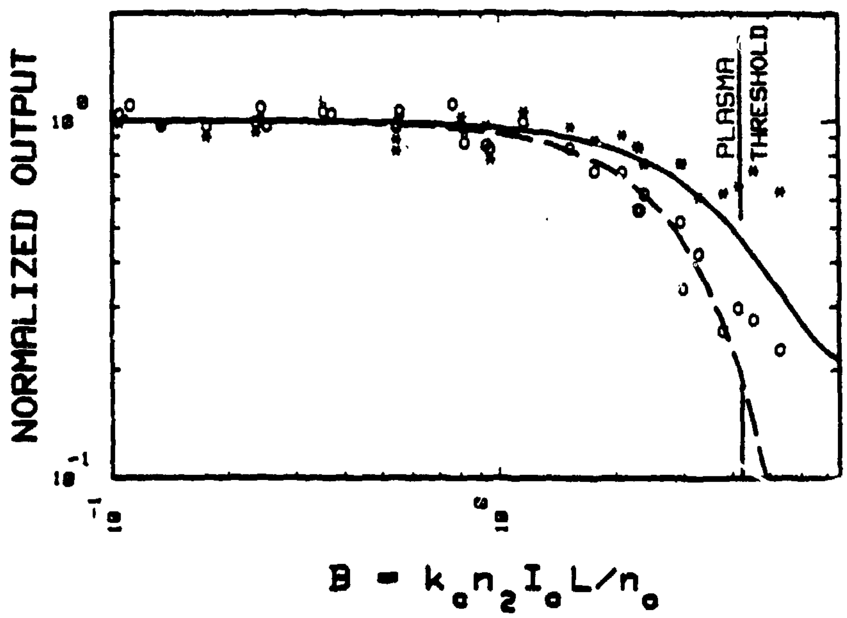

Figure 8. Measured power transmited by u_o=1 focal plane iris at input pulse peak (o) and transmitted pulse energy (*) vs B_o for 14.2 cm Ge boule. The same nonlinear index was used to fit the data in both cases, n_2 = 0.0017 cm^2/GW. The plasma formation threshold is exceeded for the last three shots on the right, causing divergence from the model.

While reviewing this data, it became clear that the temporal shape of the output pulse obtained in this configuration is probably the most sensitive indicator of small changes in nonlinear index. Figure 9 illustrates this point by showing the dramatic changes in

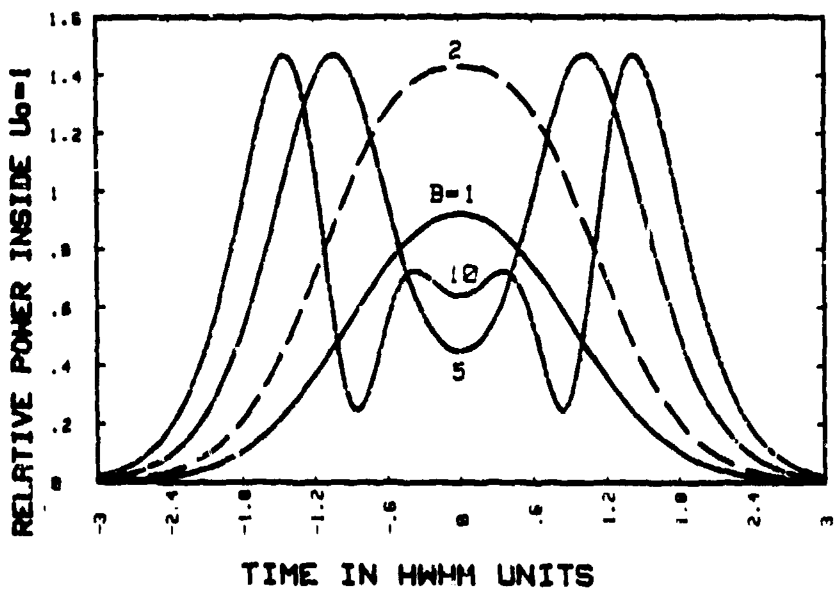

Figure 9. Calculated pulse shapes transmitted by u_o=1 focal plane iris for a Gaussian input pulse time variation, for several values of B_o. In this instance, the normalization reflects true output power, relative to the peak of the B_o=1 pulse in the absence of nonlinearities.

the power pulse through the u_o=1 iris calculated for several values of peak incident intensity when the incident pulse has a Gaussian time variation.

These predictions can be studied experimentally by comparing an observed power pulse shape transmitted by the iris to that predicted from the time-resolved laser pulse shape incident on the sample, with suitable propagation delay adjustments. This is done by letting the digitized input pulse shape drive the radial averaging calculations. Such a comparison is presented in Fig. 10 which shows the excellent agreement between the observed and predicted pulse shapes obtained with the same n_2 value used in Fig. 8, as well as the distinctly different result predicted with a 40% larger nonlinear index. In fact, 10% resolution is easily obtained with this fitting technique.

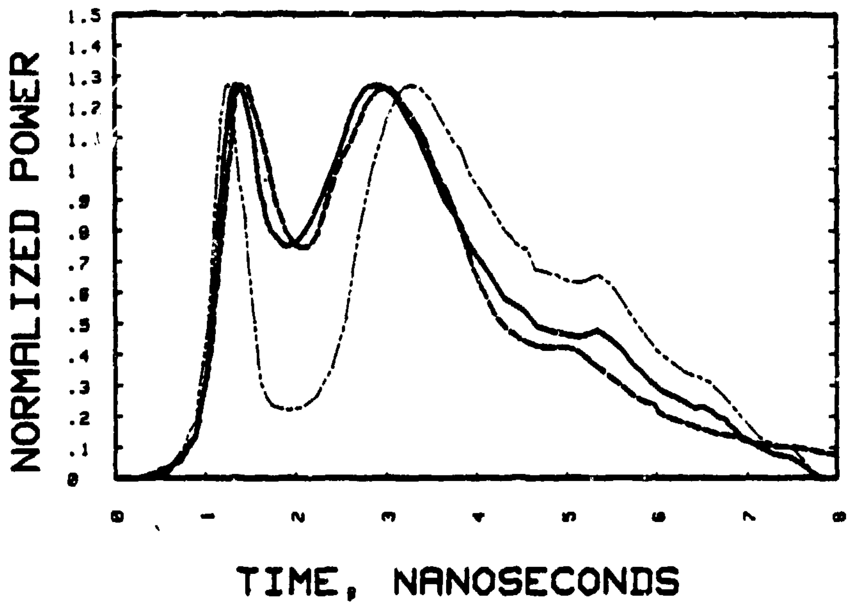

Figure 10. Predicted (dashed line) and observed (solid line) output power pulses for the conditions described in Fig. 8 when the peak incident intensity was 160 MW/cm^2, using n_2=0.0019 cm^2/GW, compared to the predicted shape for n_2=0.0027 cm^2/GW (dotted line).

Minimum sensitivity of this technique can be estimated from Fig. 5 as $n_2 = 3 \times 10^{-11}$ esu in Ge, or $n_2 = 3 \times 10^{-13}$ esu in NaCl, at CO_2 wavelengths.

Conclusions

We have reported exact analytic expressions for determining the far-field intensity distribution produced by a general hypergaussian beam in a suitably thin, transparent, optically nonlinear window. These expressions also permit analytic radial- and/or time-averaging of far-field intensities. Sufficient agreement is demonstrated between experiment and theory to justify using far-field power measurements as an adequate means of determining the nonlinear index of materials in some circumstances. Factor-of-two absolute accuracy is claimed, with 10% resolution in nonlinear index value. Sensitivity of the technique is moderately good.

References

1. An excellent review of the theory of nonlinear refraction is contained in J. H. Marburger, Prog. Quant. Electr., 4, 35 (1975).

2. R. W. Hellwarth, J. Opt. Soc. Am., 67, 1 (1977).

3. R. L. Abrams and R. C. Lind, Opt. Lett., 2, 94 (1978) and 3, 205 (1978).

4. This relationship is, of course, independent of whether one writes $\underline{E} = \mathrm{Re}\{E_1 \exp[i(kz-wt)]\}$ or $\underline{E} = 1/2\{E_1 \exp[i(kz-wt)] + c.c.\}$ In either case, $< E^2(z,t) >_t = 1/2\ E_1^2$. See, for example, C. C. Wang, Phys. Rev., 152, 149 (1966).

5. A. Yariv and D. M. Pepper, Opt. Lett. 1, 16 (1977).

6. See, for example. H. M. Smith, *Principles of Holography*, Wiley, New York (1975).

7. C. R. Phipps, Jr. and S. J. Thomas, I.E.E.E./O.S.A. Topical Conference on Inertial Confinement Fusion, San Diego, Feb. 26-28, 1980, paper WE10.

8. V. I. Bespalov and V. I. Talanov, JETP Lett. 3, 307 (1966).

9. A. Papoulis, *Systems and Transforms with Applications in Optics*, McGraw-Hill, New York (1968).

10. J. W. Goodman, *Introduction to Fourier Optics*, McGraw-Hill, New York (1968).

11. I. S. Gradshteyn and I. M. Ryzhik, *Table of Integrals, Series and Products*, Academic, New York (1965).

12. W. J. Smith, *Modern Optical Engineering*, McGraw-Hill, New York (1966).

13. A. J. Campillo, R. A. Fisher, R. C. Hyer and S. L. Shapiro, Appl. Phys. Lett., 7, 408 (1974).

14. C. R. Phipps, Jr., and S. J. Thomas, Opt. Lett. 1, 93 (1977).

15. E. McLellan, S. Stotlar, J. Webb and A. Gibbs, paper C.4, this conference.

16. D. E. Watkins, C. R. Phipps, Jr. and S. J. Thomas, Opt. Lett., to be published.

17. C. R. Phipps, Jr. and S. J. Thomas, IEEE/OSA Topical Conference on Inertial Confinement Fusion, San Diego, Feb. 26-28, 1980, paper TuB10.